Frequency stability measurement of a transfer-cavity-stabilized diode laser by using an optical frequency comb

Uetake, Satoshi; Matsubara, K.; Ito, H.; Hayasaka, K.; Hosokawa, M.

Appl. Phys. B manuscript No.
(will be inserted by the editor)

Frequency stability measurement of a transfer-cavity-stabilized diode laser by using an optical frequency comb

S. Uetake[1,2] ⋆, K. Matsubara[1], H. Ito[1], K. Hayasaka[1], M. Hosokawa[1]

[1] National Institute of Information and Communications Technology, 588-2 Iwaoka, Nishi-ku, Kobe 651-2492, Japan
[2] FAX: +81-75-753-3769, e-mail: uetake 'at' scphys.kyoto-u.ac.jp

Received: date / Revised version: date

Abstract We report results of frequency stability measurements of an extended cavity diode laser (ECDL) whose frequency is stabilized by a non-evacuated scanning transfer cavity. The transfer cavity is locked to a commercial frequency stabilized helium-neon laser. Frequency stability is measured by use of an optical frequency comb. The environmental perturbations (variations of temperature, air pressure, and humidity) are also simultaneously measured. The observed frequency drift of the ECDL is well explained by environmental perturbations. An atmospheric pressure variation, which is difficult to control with a non-evacuated cavity, is mainly affected to the frequency stability. Thus we put the cavity into a simple O-ring sealed (non-evacuated) tube. With this simple O-ring sealed tube, the frequency drift is reduced by a factor of 3, and the Allan variance reaches a value of 2.4×10^{-10}, corresponds to the frequency stability of 83 kHz, at the average time of 3000 s. Since the actual frequency drift is well estimated by simultaneous measurement of the ambient temperature, pressure, and humidity, a feed-forward compensation of frequency drifts is also feasible in order to achieve a higher frequency stability with a simple non-evacuated transfer cavity.

PACS: 42.60.By;42.60.Lh;42.55.Px

1 Introduction

It is necessary to suppress long-term frequency drifts of lasers for many applications in atomic physics. In particular, for laser cooling of ions or neutral atoms, long-term stability of less than 1 MHz is required because the cooling transition of such atoms has a natural linewidth of the order of tens of MHz. To obtain this stability, a strong atomic (or molecular) transition is often used as a frequency reference [1]. For laser cooling of alkali atoms, a cooling laser can be locked to D1 or D2 transition directly. However, such strong transitions are not always available for laser cooling of ions or short-lived radioactive species for which no atomic vapor can be used. Instead of an atomic vapor cell, a hollow-cathode lamp can be used for laser cooling of an ion (e.g. Ca^+ ion [2]). However, as described in Ref. [2], the observed signal was rather weak and the observed linewidth of 167 MHz was much broader than the natural linewidth of laser cooling transition in Ca^+ ion (22 MHz). The broadening is caused by the power and collision broadening. Because of the poor signal-to-noise ratio and the broad linewidth, it may be difficult to obtain the long-term stability of <1 MHz when the cooling laser is locked to a signal of hollow-cathode lamp.

Alternatively, a good long-term stability is obtained by transferring the stability of a frequency stabilized (master) laser to a slave laser by use of an optical transfer cavity [3–9]. In this technique, the optical path length of the transfer cavity is stabilized to the master laser. By locking the frequency of the slave laser to this cavity, the stability of the master laser can be transferred to the slave laser. When a non-evacuated transfer cavity is used, however, the absolute frequency of the slave laser changes with variations of the refractive index of air, which is a function of ambient temperature, pressure, and humidity, because of the dispersion of it. For this reason one can obtain a better stability with an evacuated cavity [6], however, such a system is complicated. A non-evacuated cavity is much simple alternative. Performance limitations of a non-evacuated cavity were discussed [9, 10]. Nevertheless, there is no direct measurement of correlations between laser frequency drift and variations of ambient conditions (temperature, pressure, and humidity).

In this paper, we investigate a long-term frequency stability of a diode laser stabilized by use of a non-evacuated scanning transfer cavity. The laser frequency is measured by using an optical frequency comb; and variations of ambient temperature, pressure and humidity are also measured simultaneously. Frequency drifts are calculated from these measured ambient conditions. The calculations are in good agreement with the measured frequency drifts. Since the variation of air pressure mainly affects the frequency drift, we put the cavity into a simple O-ring sealed tube in order to reduce a variation

⋆ *P*resent address: Department of Physics, Graduate School of Science, Kyoto University, Kyoto 606-8502, Japan

of pressure. The frequency drift is suppressed by a factor of 3 by using this simple, non-evacuated O-ring sealed tube.

2 Performance limitations in a non-evacuated transfer cavity

We use a scanning transfer cavity and a commercial frequency-stabilized He-Ne laser in order to stabilize frequency of a slave laser. In each scan of the transfer cavity, a transmission peak position of the slave laser relative to that of the master laser is detected, as depicted in Fig. 1 (b). The relative position of the slave laser is kept constant by a servo-control system. As mentioned above, the absolute frequency of the slave laser changes with varying the refractive index of air.

In order to introduce the dependence of frequency on the refractive index of air, we start from the resonant condition of the confocal Fabry–Perot cavity. The resonant condition of two adjacent modes of master laser are given by

$$N_m \lambda_m = 2 n_m L_0, \tag{1}$$

$$\left(N_m + \frac{1}{2}\right) \lambda_m = 2 n_m (L_0 + \Delta L_0), \tag{2}$$

and a transmission peak of the slave laser located between two peaks of the master laser is

$$N_s \lambda_s = 2 n_s (L_0 + \alpha \Delta L_0), \tag{3}$$

where N is the mode number, λ is the wavelength, n is the refractive index of air, L_0 is the spacing between the mirrors, ΔL_0 is the difference of the cavity length between two transmission peaks of master laser shown in Fig. 1 (b), α is an arbitrary number ($0 < \alpha \leq 1$), and the subscript m (s) denotes master (slave) laser. From Eqs. (1)–(3), we obtain the relation between the wavelengths of the slave laser and the master laser

$$\lambda_s = \lambda_m \frac{2N_m + \alpha}{2N_s} \frac{n_s}{n_m}. \tag{4}$$

Thus the maximum relative fluctuation of λ_s can be written as the sum of three terms:

$$\left|\frac{\delta\lambda_s}{\lambda_s}\right| \leq \left|\frac{\delta\lambda_m}{\lambda_m}\right| + \left|\frac{\delta\alpha}{2N_m + \alpha}\right| + \left|\frac{\delta n_s}{n_s} - \frac{\delta n_m}{n_m}\right|. \tag{5}$$

The second and the third term of Eq. (5) are residual drifts: if one can reduce these two terms, the stability of the master laser can be transferred to the slave laser.

The second term of Eq. (5) corresponds to a residual locking error and a spectral resolution of the system. It is important to increase the spectral resolution in order to achieve better stability in a scanning transfer cavity scheme, because frequency fluctuations smaller than the spectral resolution cannot be detected. In the present system, the spectral resolution is determined by (a) an analog resolution (i.e. a full-width at half-maximum (FWHM) of the cavity transmission peaks), (b) a digital resolution (i.e. a number of sampling data points), and (c) a signal-to-noise ratio (SNR) of the detector. In the present system, the FWHM is 7.5 MHz, the number of data points between two peaks of master laser (300 MHz) are around 1200, and the SNR is about 24. The resolution of the present system is estimated to be ∼500 kHz.

Table 1 The dependence of the frequency stability on temperature, pressure, and humidity. The conditions for the calculation are $T = 25\,^{\circ}\mathrm{C}$, $P = 1013.25$ hPa, $h = 50\%$.

$\lambda_m,\ \lambda_s$ [nm]	$(\delta\nu_s)_T$ [MHz/°C]	$(\delta\nu_s)_P$ [MHz/hPa]	$(\delta\nu_s)_h$ [MHz/%]
633, 866	−1.9	0.61	0.051

The refractive index of air $n(\lambda, T, P, f)$ depends on λ, the temperature T, the total air pressure P, and the partial pressure f of water vapor [11]. Thus the third term of Eq. (5) does not become zero and this gives a limitation in the case of non-evacuated cavity, as discussed in Ref. [9, 10]. Variations of $\delta\lambda$, δT, δP, and δf lead a variation of the refractive index of air δn:

$$\delta n = \frac{\partial n}{\partial \lambda}\delta\lambda + \frac{\partial n}{\partial T}\delta T + \frac{\partial n}{\partial P}\delta P + \frac{\partial n}{\partial f}\delta f. \tag{6}$$

The first term of Eq. (6) can be neglected because fluctuations in laser wavelength $\delta\lambda$ is much smaller than other fluctuations in δT, δP, and δf during the experiment. Therefore

$$\frac{\delta n_s}{n_s} - \frac{\delta n_m}{n_m} \simeq \beta_T \delta T + \beta_P \delta P + \beta_f \delta f, \tag{7}$$

where

$$\beta_X = \frac{1}{n_s}\frac{\partial n_s}{\partial X} - \frac{1}{n_m}\frac{\partial n_m}{\partial X},$$

and X denotes T, P, or f. For convenience, we use the relative humidity $h = 100 f/e(T)$, where $e(T)$ is saturation vapor pressure of water, instead of f. Then we finally obtain a frequency fluctuation of slave laser $\delta\nu_s$ corresponds to the third term of Eq. (5):

$$\delta\nu_s \approx -\nu_s \frac{\delta\lambda_s}{\lambda_s} = (\delta\nu_s)_T \delta T + (\delta\nu_s)_P \delta P + (\delta\nu_s)_h \delta h, \tag{8}$$

where

$$\begin{aligned}
(\delta\nu_s)_T &= -\nu_s \left[\left(\frac{1}{n_s}\frac{\partial n_s}{\partial T} - \frac{1}{n_m}\frac{\partial n_m}{\partial T}\right)\right. \\
&\qquad \left. + \frac{h}{100}\frac{de(T)}{dT}\left(\frac{1}{n_s}\frac{\partial n_s}{\partial f} - \frac{1}{n_m}\frac{\partial n_m}{\partial f}\right)\right], \\
(\delta\nu_s)_P &= -\nu_s \left(\frac{1}{n_s}\frac{\partial n_s}{\partial P} - \frac{1}{n_m}\frac{\partial n_m}{\partial P}\right), \\
(\delta\nu_s)_h &= -\nu_s \frac{e(T)}{100}\left(\frac{1}{n_s}\frac{\partial n_s}{\partial f} - \frac{1}{n_m}\frac{\partial n_m}{\partial f}\right).
\end{aligned} \tag{9}$$

We calculate the coefficients (9) by using the updated Edlén equation for $n(\lambda, T, P, f)$ [12] and the formula for $e(T)$ by Sonntag [13, 14]; the results are listed in Table 1.

3 Experimental setup

The schematic diagram of the laser frequency stabilization system is shown in Fig. 1 (a). We used a commercial stabilized He-Ne laser system (Melles Griot 05 STP 905) as a master laser. A typical frequency drift is ± 1.2 MHz for eight hours. The slave laser is a grating stabilized extended cavity diode laser (ECDL: TOPTICA DL100) whose wavelength is 866 nm. These lasers (orthogonally polarized) are coupled into the transfer cavity.

A confocal Fabry–Perot cavity is used as a transfer cavity. The cavity is made of a bored INVAR rod. A ring PZT (Piezomechanik HPSt 150/14-10/12) and two mirrors are attached to the ends of the rod. The mirror reflectance is 99% at 633 nm and 866 nm. The transfer cavity has a free-spectral range (FSR) of 300 MHz and a finesse of about 40. Transmission peaks are detected independently by use of a polarizing beam splitter and two photodiodes. The detected signals are sent to the computer. Figure 1 (b) shows the typical cavity transmission peaks.

For data acquisition and feedback control, we use a 12-bit analog-to-digital converter (ADC) board (Interface Corp. PAZ-3163) and a 12-bit digital-to-analog converter (DAC) board (Interface Corp. PAZ-3338). The ADC board has two input channels and a 512K sampling buffer memory for each channel; the sampling rate is up to 10 mega-samples per second (MSa/s). Data acquisitions are synchronized with cavity scan. In each scan, the computer detects master and slave laser's peak positions. In order to compensate thermal drifts of the cavity length, the present peak position of the master laser is compared to the previous one. Then the computer sends a signal to the cavity PZT so that the peak position is kept constant. Then it compares $\alpha \Delta L_0$ to the previous one, and sends a signal to the PZT of the ECDL so that α is kept constant. Since the maximum correction rate of a frequency drift is determined by the cavity scan speed, it is important to increase the scan speed as fast as possible in order to achieve higher frequency stability [5]. In the present system, the PZT is scanned by a triangular wave derived from a frequency synthesizer running at a frequency of 1 kHz. The scan rate is limited by a frequency response of the PZT.

The ambient conditions are measured using three sensors: a platinum resistance temperature sensor, a silicon Piezo-resistive pressure sensor (Fujikura XFPM-115KPA), and a humidity sensor (Honeywell HIH-3610-003). The output voltages of sensors are recorded by a data logger. The resolutions of temperature, pressure, and humidity are 0.1 °C, 0.2 hPa, and 0.03%RH (relative humidity) respectively; these are determined by the voltage resolutions of the data logger.

The optical frequency measurements are carried out by using a commercial optical frequency comb (Menlo FC8003). The beat signal between one of the comb mode and the slave laser is measured by the frequency counter whose gate time is 1 s. The frequency counters and the rf synthesizers for the optical frequency comb are referenced to the 10 MHz output of a hydrogen-maser.

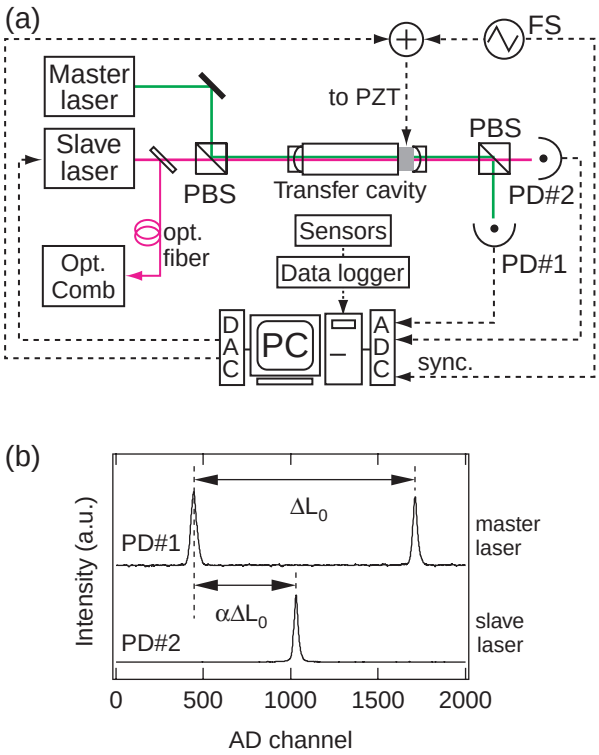

Fig. 1 (a) Schematic diagram of the apparatus. The master and the slave lasers (orthogonally-polarized) are coupled into the transfer cavity through polarizing beam splitter (PBS). The cavity PZT is scanned by function synthesizer (FS). The transmission peaks are detected by photodiodes (PD); then the signal is sent to the computer (PC). The ambient temperature, pressure, and humidity are measured by using sensors with a data logger. The optical frequency is measured by an optical frequency comb. Timing of data acquisition is synchronized with scanning of the cavity. Solid lines represent the optical paths; dashed lines represent electrical connections. (b) Typical cavity transmission spectrum.

4 Measurement of frequency drift

4.1 Frequency drifts measurement under the non-evacuated cavity system

We first measured the frequency drift of the ECDL stabilized by the non-evacuated cavity system. The absolute frequency drifts of slave laser ($\lambda_s = 866$ nm) were measured for two hours. The results are shown in Fig. 2. The peak-to-peak variations of the ambient pressure, temperature, and humidity are 1.8 hPa, 0.2 °C, and 0.5% respectively, as shown in Fig. 2 (a). Figure 2 (b) shows the residual locking error, which is converted into frequency units by use of the equation: (error)$= \alpha \times 633/866 \times 300$ MHz. The peak-to-peak drift of the residual error is 80 kHz. The drift is caused by imperfections of the servo control. This can be reduced by increasing the low-frequency gain of the servo control system. The black line in Fig. 2 (c) shows the measured drift of the beat signal.

While there are only small variations in the temperature and the humidity, the pressure varies considerably. Atmospheric pressure cannot be controlled under the non-evacuated

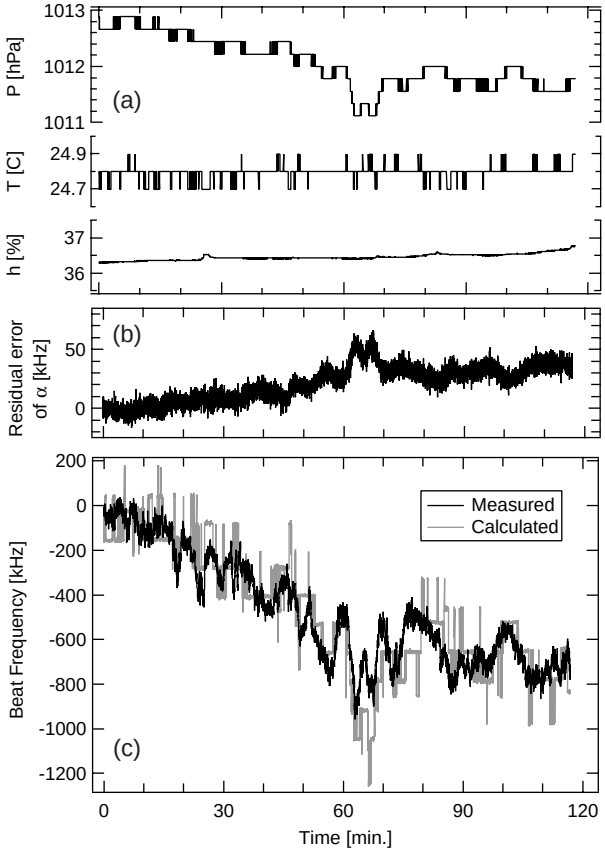

Fig. 2 Frequency drifts measurement with the non-evacuated transfer cavity system. (a) Results of ambient condition measurement. The temperature and the humidity variations are sufficiently small ($0.2\,^{\circ}$C and 0.5%) in our laboratory, while the change of pressure is slightly large (1.8 hPa peak-to-peak). Pressure changes cannot be controlled by the non-evacuated cavity. (b) Residual locking error. $\delta\alpha$ is converted into frequency units. The variation of error is 80 kHz (peak-to-peak). (c) The beat frequency drift as a function of time. The calculated frequency drift (the gray line) is in good agreement with the measured one (the black line). Beat frequency is measured by optical frequency comb and the frequency counter whose gate time is 1 s.

cavity system. Thus the frequency drift is mainly caused by the pressure change.

We calculate frequency drifts by using the coefficients in Table 1, the measured environmental parameters (temperature, pressure, and humidity), and residual locking error. The gray line in Fig. 2 (c) shows the calculated frequency drift; it is in good agreement with the measured one.

4.2 Frequency drifts measurement under the O-ring sealed cavity system

From the results described in the previous section, one can improve the frequency stability by reducing variations of atmospheric pressure. For this purpose, we made an O-ring sealed aluminum tube and the cavity is placed into the tube. The tube is also not evacuated for simplicity. Wedge glass plates are used as view ports of the tube.

The results are shown in Fig. 3. This time the ambient pressure increases monotonically; the variations of pressure, temperature, and humidity is 1.4 hPa, $0.2\,^{\circ}$C, and 2.8%, respectively. Figure 3 (b) shows the residual locking error. The peak-to-peak drift of the residual error is 90 kHz.

There is a significant difference between the actual frequency drift (the black line in Fig. 3 (c)) and the calculated one (the gray line). The average calculated drift is 380 kHz/h, while the measured one is 120 kHz/h. The residual drift seems to be caused by two reasons: the drift of the master laser and the leakage of air from the tube. We cannot distinguish these two effects, because the typical frequency drift of the master laser is ± 1.2 MHz for 8 hours, and this is of the same order as the measured drift. Although a small residual drift remains, the actual frequency drift is a factor of 3 smaller than the calculated one. This shows that a simple O-ring sealed tube is sufficient to suppress pressure changes inside the tube, and hence to suppress frequency drifts caused by ambient pressure variations.

4.3 Allan variance

We calculate the Allan variance to characterize the frequency stability of the laser. The square root of Allan variances $\sigma(\tau)$ of the measured beat frequencies are plotted in Fig. 4, together with that of the free-running ECDL and the master laser. $\sigma(\tau)$ of the stabilized lasers (curves A and B: solid line with triangles and squares) are approximately one to two orders of magnitude less than that of the free-running ECDL (solid line with circles) for all time range. $\sigma(\tau)$ of the curve A is 8.3×10^{-10} at 3000 s and that of the curve B is 2.4×10^{-10} at 3000 s. The corresponding long-term frequency stabilities are 290 kHz in the non-evacuated cavity case, and 83 kHz in the O-ring sealed cavity case. The magnitude of the curve A is larger than that of the master laser's curve by a factor between 2 and 4 for the time range longer than 10 s. On the other hand, that of curve B is close to that of the master laser's curve. Thus the stability of the master laser is almost transferred to the slave laser.

5 Discussion

We calculate the coefficients in Eq. (9) for a slave laser wavelength of 390 nm to 900 nm. Here we assume the updated Edlén equation can be used up to 900 nm. For this calculation, we choose the wavelengths of master laser to 405 nm, 422 nm, 507 nm, 532 nm, 633 nm, and 780 nm. The results are plotted in Fig. 5. Obviously, slopes of curves become steep at short wavelength. This is due to large dispersion of the refractive index of air. Thus the choice of the master laser wavelength is important to minimize a frequency change due to dispersion. In addition, a temperature change strongly affects frequency stability. However, the temperature can be easily controlled within $0.5\,^{\circ}$C. Then, the factor that is impossible to eliminate is the pressure change in the system with a non-evacuated cavity. As mentioned in the previous section,

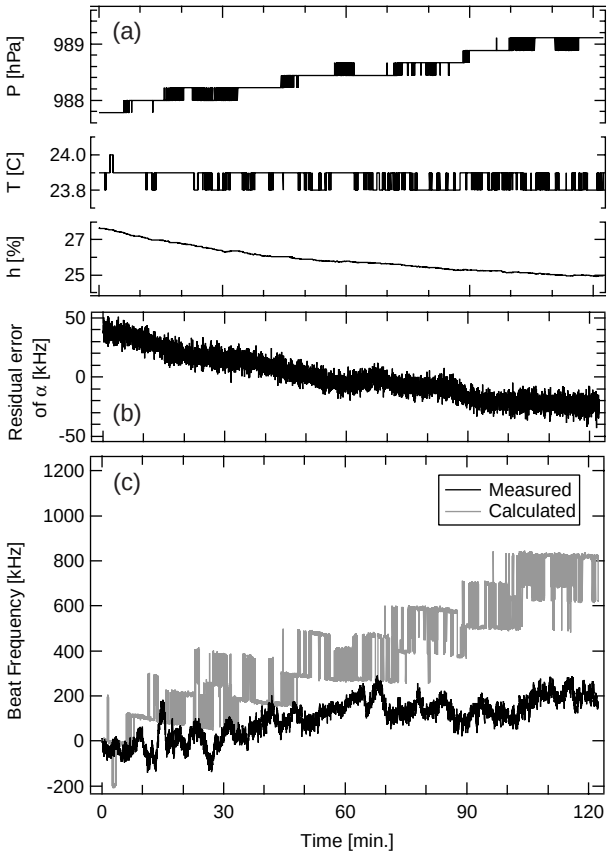

Fig. 3 Frequency drifts measurement with the O-ring sealed transfer cavity system. (a) Results of ambient (outside of the O-ring sealed tube) condition measurement. The temperature and the humidity variations are also sufficiently small (0.2 °C, 2.8%). The peak-to-peak change of pressure is 1.3 hPa. (b) Residual locking error. $\delta\alpha$ is converted into frequency units. The change of error is 90 kHz (peak-to-peak). (c) The beat frequency drift as a function of time. The black line is the measured frequency change; the gray line is the calculated frequency change. There is a significant difference between two lines. The results show that the pressure change inside the O-ring sealed tube was suppressed.

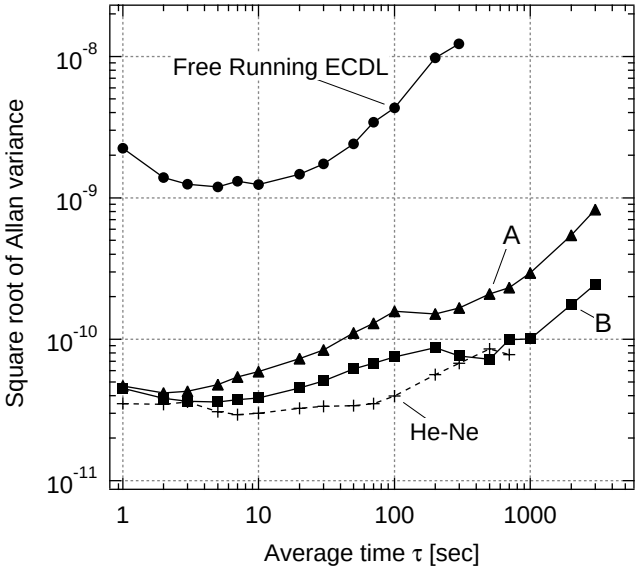

Fig. 4 Square root of Allan variance of the beat frequency between the comb and the laser stabilized by (A) open transfer cavity system and (B) hermetic sealed transfer cavity system. The solid line with circle is for the measured frequency of free-running ECDL; the broken line with '+' markers is for that of the master (He-Ne) laser.

a simple O-ring sealed cavity is a better alternative in order to reduce a pressure change.

We show several combinations of master and slave laser wavelengths to obtain 1 MHz stability as examples. In the subsequent discussion, we suppose a situation that is a temperature change of 0.5 °C, a pressure change of 2 hPa, and a humidity change of 10%. For slave lasers between 397 nm and 433 nm, a diode laser locked to the atomic lines of potassium (405 nm) or rubidium (422 nm) is suitable. These atomic lines are recently investigated for stabilization of GaN diode lasers [15,16]. By choosing the master laser of 405 nm (422 nm), 1 MHz stability is obtained for a slave laser from 397 nm to 414 nm (412 nm to 433 nm). For slave lasers around 500 nm to 700 nm, an iodine-stabilized laser is suitable as a master laser. Iodine molecule lines can be used to stabilize a frequency-doubled diode laser at 507 nm [17], a frequency-doubled Nd:YAG laser at 532 nm [18], or a He-Ne laser at 633 nm. These lasers can be used for slave lasers at 486 nm to 533 nm, 507 nm to 564 nm, or 587 nm to 707 nm, respectively. For slave lasers in near-infrared region (686 nm to 900 nm), a diode laser locked to the rubidium line (780 nm) is suitable.

The conditions considered in these examples are worse than those in the experiments described in the previous section. With better stabilities of ambient conditions, one can easily obtain higher frequency stability (or wider wavelength range of slave lasers). By choosing an appropriate wavelength of master laser and achieving sufficient stabilities of ambient conditions, the long-term stability of <1 MHz is feasible. Therefore the method demonstrated in this paper is suitable for various atomic physics experiments with alkali-like ions, alkaline-earth like atoms, or group-III atoms: such as Ca^+ (397 nm and 866 nm) [8, 19], Yb (399 nm, 404 nm, 649 nm, 770 nm) [20], Ga (403 nm, 417 nm) [21, 22], or In (410 nm, 451 nm) [23].

Another way to achieve higher long-term stability is a 'feed-forward compensation' of the slave laser frequency. Results in section 4.1 show that a real-time compensation of the actual frequency drift is feasible by simultaneous measurement of temperature, pressure and humidity. The computer subtracts the estimated frequency drift from control signal of the PZT of the ECDL. With this feed-forward compensation, it is feasible to achieve a better stability even if one uses a non-evacuated cavity. In order to estimate long-term stability of a feed-forward compensated system, we calculate the Allan variance by use of the difference between the measured frequency data and the calculated one in the section 4.1. $\sigma(\tau)$ of the difference reaches 1.0×10^{-10} at 3000 s, which corresponds to 35 kHz. Although the present resolution of the temperature and the pressure is insufficient for this feed-forward

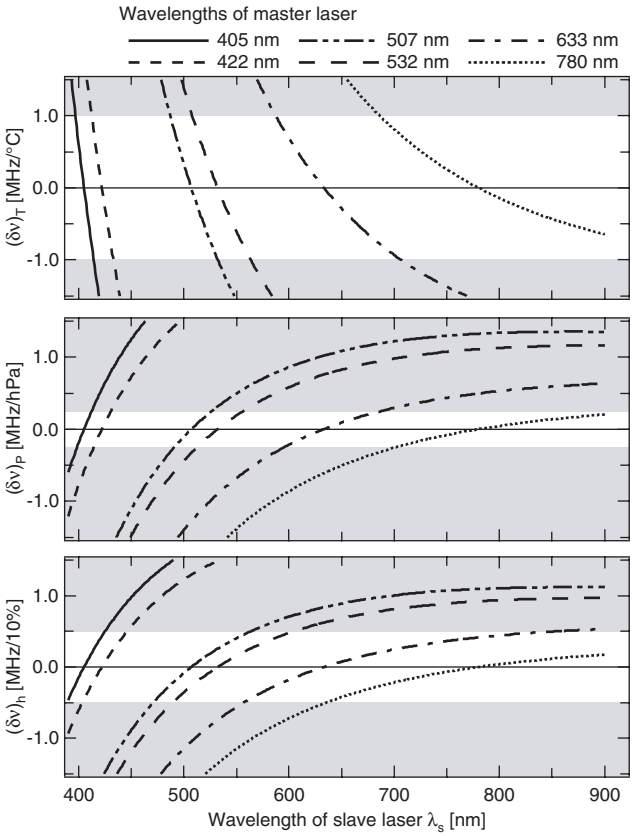

Fig. 5 The dependence of frequency on temperature, pressure, and humidity changes (coefficients in Eq. (9)) as a function of the wavelength of salve laser. White areas show acceptable wavelength ranges of slave lasers to obtain 1 MHz stability with conditions of a temperature change of 0.5 °C, a pressure change of 2 hPa, and a humidity change of 10%.

compensation, it is limited by the voltage resolution of the data logger. It is easy to increase the resolution by replacing the data logger with another one. Thus long-term frequency stability of <100 kHz is attainable by using a non-evacuated cavity and a feed-forward compensation of the frequency.

6 Conclusions

We have measured the absolute frequency drift of an extended-cavity diode laser that is stabilized by use of a non-evacuated transfer cavity and a commercial stabilized He-Ne laser. The frequency drift is measured by an optical frequency comb. The ambient temperature, pressure and humidity are simultaneously measured. From measured ambient conditions, frequency drifts caused by changes in the refractive index of air is calculated. The calculated frequency drift in the non-evacuated cavity system is in good agreement with the measured one. Long-term frequency drifts are mainly caused by changes of ambient pressure in the non-evacuated transfer cavity system. By putting the cavity into a simple O-ring sealed tube, drifts are suppressed by a factor of 3. The square root of Allan variance of the laser frequency stabilized by this O-ring sealed cavity is 2.4×10^{-10} at 3000 s, which corresponds to the frequency stability of 83 kHz. The value is approximately one to two orders of magnitude less than that of the free-running ECDL. By use of a O-ring sealed cavity, the stability of the master laser is almost transferred to that of the slave laser. The dependence of the frequency on temperature, pressure, and humidity is calculated for a slave laser wavelength of 390 nm to 900 nm. We discuss a possibility of a feed-forward frequency compensation to obtain a higher frequency stability with a simple non-evacuated transfer cavity.

References

1. J. L. Hall, L. Hollberg, T. Baer, and H. G. Robinson, Appl. Phys. Lett. **39**, 680 (1981).
2. R. Ohmukai, M. Watanabe, H. Imajo, K. Hayasaka, and S. Urabe, Jpn. J. Appl. Phys. **33**, 311 (1994).
3. J. Helmcke, S. A. Lee, and J. L. Hall, Appl. Opt. **21**, 1686 (1982).
4. B. G. Lindsay, K. A. Smith, and F. B. Dunning, Rev. Sci. Instrum. **62**, 1656 (1991).
5. S. M. Jaffe, M. Rochon, and W. M. Yen, Rev. Sci. Instrum. **64**, 2475 (1993).
6. W. Z. Zhao, J. E. Simsarian, L. A. Orozco, and G. D. Sprouse, Rev. Sci. Instrum. **69**, 3737 (1998).
7. A. Rossi, V. Biancalana, B. Mai, and L. Tomassetti, Rev. Sci. Instrum. **73**, 2544 (2002).
8. K. Matsubara, S. Uetake, H. Ito, Y. Li, K. Hayasaka, and M. Hosokawa, Jpn. J. Appl. Phys. **44**, 229 (2005).
9. P. Bohlouli-Zanjani, K. Afrousheh, and J. D. D. Martin, Rev. Sci. Instrum. **77**, 093105 (2006).
10. E. Riedle, S. H. Ashworth, J. J. T. Farrell, and D. J. Nesbitt, Rev. Sci. Instrum. **65**, 42 (1994).
11. B. Edlén, Metrologia **2**, 71 (1966).
12. K. P. Birch and M. J. Downs, Metrologia **30**, 155 (1993).
13. D. Sonntag, Meteorol. Zeitschrift **3**, 51 (1994).
14. WMO Guide to Meteorological Instruments and Methods of Observation, 7th ed.
15. S. Uetake, K. Hayasaka, and M. Watanabe, Jpn. J. Appl. Phys. **42**, L332 (2003).
16. K. Hayasaka, Opt. Commun. **206**, 401 (2002).
17. A. Yamaguchi, S. Uetake, and Y. Takahashi, Appl. Phys. B **91**, 57 (2008).
18. F.-L. Hong, J. Ishikawa, Z.-Y. Bi, J. Zhang, K. Seta, A. Onae, J. Yoda, and H. Matsumoto, IEEE Trans. Instrum. Meas. **50**, 486 (2001).
19. K. Matsubara, K. Hayasaka, Y. Li, H. Ito, S. Nagano, M. Kajita, and M. Hosokawa, Appl. Phys. Express **1**, 067011 (2008).
20. S. Uetake, A. Yamaguchi, D. Hashimoto, and Y. Takahashi, Appl. Phys. B **93**, 409 (2008).
21. O. M. Marago, B. Fazio, P. G. Gucciardi, and E. Arimondo, Appl. Phys. B **77**, 809 (2003).
22. O. N. Prudnikov and E. Arimondo, J. Opt. Soc. Am. B **20**, 909 (2003).
23. H. Leinen, D. Gläßner, H. Metcalf, R. Wynands, D. Haubrich, and D. Meschede, Appl. Phys. B **70**, 567 (2000).